Applied Thermal Engineering 138 (2018) 731–739

Contents lists available at ScienceDirect

Applied Thermal Engineering

journal homepage: www.elsevier.com/locate/apthermeng

Research Paper

A pressure drop study for packed bed adsorption thermal energy storage

Behzad Baghapour, Mina Rouhani, Amir Sharafian, Sahand Behboodi Kalhori, Majid Bahrami*

Laboratory for Alternative Energy Conversion (LAEC), School of Mechatronic Systems Engineering, Simon Fraser University, BC V3T 0A3, Canada

HIGHLIGHTS

- Experimental and modeling study is performed on pressure drop inside adsorber beds.
- The model covers a wide range of porosity, from low to high permeability medium.
- A modified permeability is defined to consider inertial effects.
- The experiment reveals negligible effect of water uptake on pressure drop.
- The model shows slight change in pressure drop due to heat of adsorption.

ARTICLE INFO

Keywords:
Pressure drop
Adsorption packed bed
Inertial effect
Modified permeability
Thermal energy storage

ABSTRACT

Adsorption thermal energy storage has received considerable attention as it can overcome the mismatch between supply and demand of renewables, providing high energy storage per volume. In the packed bed adsorption thermal energy storage, pressure drop is of key concern since higher pressure drop leads into lower energy storage efficiency. In this paper, an experimental and modeling investigation on the pressure drop inside the adsorption packed beds is performed. An accurate semi-analytical closed-form relationship is proposed to calculate the pressure drop inside a column of adsorbent materials, taking into account the Laplacian friction, as well as the inertial effects. The model covers a wide range of porosity, between low-permeability medium, a dense packed bed of spherical particles, and high-permeability media, a pure viscous fluid. A modified permeability is defined to consider the inertial effect for a moderate range of the particle Reynolds number ($0 < Re_p < 300$). An experimental apparatus is designed for measuring the pressure drop for different bed sizes and inlet air velocities. The proposed model shows good agreement with the experimental data with the relative difference of 7.6% at 0.73 m/s for silica gel and 15.3% at 0.84 m/s for zeolite 4A packed beds. The experiment reveals that the effect of water uptake on the pressure drop of packed bed with wet adsorbent is negligible in the tested particle Reynolds number range, with a relative difference of less than 1.0% compared to dry adsorbent for 18–30 cm long columns. The proposed formula for pressure drop, consequently, can be applicable for wet adsorbents regardless of the water uptake amount, with a good level of accuracy. Moreover, the analytical model shows up to ± 2% change in pressure drop due to heat of adsorption of the tested adsorber columns.

1. Introduction

Packed beds are widely used in various applications such as gaseous mixture drying [1], purification processes [2], dehumidification [3], filtration [4], adsorption cooling systems [5], and thermal energy storage systems [6,7], to name a few. The significant energy consumption for overcoming the pressure drop in packed beds, makes the optimal design of such systems crucial. Particularly, pressure drop is of great importance for energy storage efficiency of the sensible [8], latent [9], and packed bed thermal energy storage (TES) systems [10].

Adsorption TES (ATES) is a promising sustainable, energy efficient alternative to conventional heating and cooling methods, with a high energy storage density and insignificant heat loss for long-term storage [11]. Performance of the open ATES highly depends on diffusion of adsorbate inside the bed, heat transfer, and pressure drop [12–14]. High pressure drop in ATES results in the use of electric fans, which increases the power consumption, and consequently decreases the energy storage efficiency [15]. This makes detailed study of pressure drop in the adsorber bed and optimum design of the bed crucial to promote widespread adoption of open ATES.

Empirical correlations for different packing geometries [16–18] as well as analytical models of linear Darcy flow problems [16] are

* Corresponding author.
E-mail address: mbahrami@sfu.ca (M. Bahrami).

https://doi.org/10.1016/j.applthermaleng.2018.03.098
Received 3 January 2017; Received in revised form 18 February 2018; Accepted 29 March 2018
Available online 31 March 2018
1359-4311/

Nomenclature

A	cross-sectional area
C	coefficient of the inertial effect (m^{-1})
D	Bed's diameter (m)
ESD	energy storage density
e, E	linearization error
d_p	particle diameter (m)
f''_p	porous bulk friction
K	permeability (m^2)
$\widetilde{K}$	modified permeability (m^2)
H	Bed height (m)
ΔP	pressure drop (Pa)
$\mathscr{Q}$	volumetric flow rate (m^3/s)
Re_p	particle Reynolds number
RH	relative humidity
T	temperature (°C)
u	macroscopic fluid velocity (m/s)
U_0	average velocity (m/s)
x,r	spatial coordinates (m)
w_{max}	maximum water uptake

Greek symbols:

α,β	coefficients in modeling porous friction
ξ,η	non-dimensional spatial coordinates
ε	porosity
ρ	density of the fluid (kg/m^3)
μ	dynamic viscosity of the fluid ($N\,s/m^2$)
$\widetilde{\mu}$	effective viscosity ($N\,s/m^2$)
τ_f	viscous friction tension (N/m^2)
λ	parameter regarding non-dimensional permeability
σ	pressure-drop scaling factor
ψ	friction factor
ϕ	approximating variable in linearization approach
CF	cost function (Eq. (31))

Sub/Superscripts:

p	Particle
f	Fluid
cv	Control volume
pf	Porous friction
vf	Viscous friction
$*$	Non-dimensional value

available for pressure drop calculations. However, non-linearity of the inertial effects limits the theoretical investigations to the numerical methods [19]. Although the numerical approaches present comparative accurate results for laminar and turbulent flows [20–23], high computational costs decrease their applicability for complex designs. Accurate analytical model provides an easy-to-use relationship for the pressure drop calculation. The main focus of analytical studies was mainly on deriving viscous permeability based on the Stokes flow at the pore-scale [24,25]. Brinkman [26] modified the Darcy's equation by adding the viscous diffusion effect. He showed that the effective viscosity, in essence, is a function of the fluid dynamic viscosity, and the packed bed porosity and tortuosity [26]. Neale and Nader [27] developed a permeability correlation using a drag force model over a single particle embedded on swarm of particles.

The non-linearity, due to high flow speed, was introduced by Ergun in the pressure drop calculations of packed beds [18]. Moreover, the effect of porosity variation was taken into account in the pressure drop calculation of packed beds with low bed-to-particle diameter ratios, by correcting the Ergun's equation [28,29].

Packed bed thermal energy storage systems have been investigated by experiments [12,30], lumped element numerical model [31], and computational fluid dynamics (CFD) [32]. Complexity of the numerical simulation of reacting flow [33] can be favorably reduced by using semi-analytical approaches for the adsorber packed beds [3,34]. For adsorption dehumidification application, Finocchiaro et al. [30] found that the incoming air temperature has a slight impact on the pressure drop inside the packed beds. They also showed that the Ergun's equation could predict pressure drop with about 20% relative difference, for the flowrate range of 100–500 m^3/h, while it was less accurate for higher air flowrates.

In this study, a theoretical-experimental approach is followed to study the steady-state axisymmetric fully-developed flow inside the cylindrical adsorption packed beds. A new compact analytical model is developed with consideration of viscous friction, viscous permeability, and the inertial effect, to calculate the pressure drop. A testbed of adsorbent is designed and built, and several pressure drop measurements

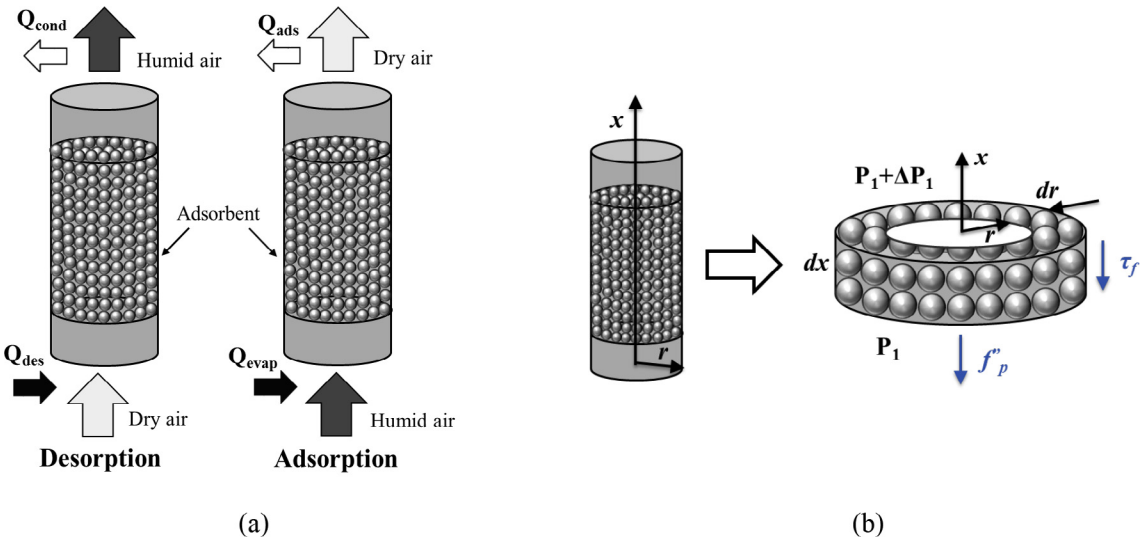

Fig. 1. (a) Open adsorption thermal energy storage [35] and (b) schematic of acting friction tensions on a control volume of a cylindrical packed bed.

through the test column are conducted. The effect of uptake on the pressure drop inside the adsorption packed bed is also analyzed. The model capability to predict pressured drop in the packed beds with a wide range of permeability is examined with the existing experimental data. Moreover, the governing equations of a steady-state incompressible isothermal flow are solved by using CFD and the results are compared with the results of the proposed model. good agreements between both experimental and numerical results with the proposed analytical results have been observed.

2. Open thermal energy storage system

The schematic diagram of an open adsorption TES is shown in Fig. 1(a). During charging process, dry hot air passes through an adsorber packed bed, leaving the bed cold and humid. After desorption, ATES can remain charged as long as no adsorbate is introduced into the bed. In Adsorption process, bed is discharged by adsorbing water vapour from cold humid air and releasing heat of adsorption to the air [35]. This heat, which is a combination of the latent and binding heat, can be used for heating purpose.

Freni et al. [36] showed that for adsorption cooling system (ACS), the loose grain packed bed adsorber provides more volumetric power compared to the coated adsorber bed. In the open ATES systems, energy storage per volume is higher for the packed bed adsorbers . Although, one of the drawbacks of the loose grain adsorption system compared to the coated adsorber bed is the pressure drop through the packed adsorbent materials, which suppresses the adsorbate diffusion [37] and reduces the storage efficiency.

3. Pressure drop model development

A schematic of a cylindrical granular bed and the acting friction tensions over a representative control volume are shown in Fig. 1(b). The following assumptions are considered:

- The fluid flow is steady-state, laminar, fully-developed, and axisymmetric.
- The fluid properties remain constant along the adsorption packed bed.
- Temperature change due to adsorption has negligible effect on the pressure drop.
- The gravity effect is neglected.
- The porosity is uniform inside the bed (the effect of confining wall on the porosity distribution has been neglected in low bed-to-particle diameter ratios [28]).

Using the above assumptions, the force balance on each control volume leads to:

$$\frac{dP}{dx} = \frac{1}{r}\frac{d}{dr}(r\tau_f) - f_p'' \tag{1}$$

where the first and second terms on the right-hand side of the equation are the viscous friction acting on the surface of the control volume, and the porous friction that imposed on the volume, respectively.

Since a fully-developed flow is assumed, the velocity profile is not a function of the axial direction and the pressure gradient is constant along the bed. Therefore, the overall pressure drop can be calculated only by summing up the pressure drops of all the control volumes. Consequently, the pressure drop of each control volume of unit length can be rewritten as follows:

$$(\Delta P)_{cv} = (\Delta P)_{vf} + (\Delta P)_{pf} \tag{2}$$

where $(\Delta P)_{vf}$ is the pressure loss due to the viscous drag force from surrounding fluid on the surface of the control volume and $(\Delta P)_{pf}$ is the effect of porous drag force exerted on the bulk of the control volume. Considering a Newtonian fluid, *i.e.*, $\tau_f = \widetilde{\mu}(du/dr)$, the viscous-drag term can be formulated as follows:

$$(\Delta P)_{vf} = \widetilde{\mu}\left(\frac{d^2u}{dr^2} + \frac{1}{r}\frac{du}{dr}\right) \tag{3}$$

where $\widetilde{\mu}$ is the effective dynamic viscosity, defined as $\widetilde{\mu}/\mu = 1/\varepsilon$ for an isotropic porous medium [38].

The porous friction contribution in the pressure drop calculation has two main parts: i) a linear viscous permeability term, assuming a creeping flow in the pore-scale, and ii) a nonlinear inertial term due to the high particle Reynolds numbers. The overall porous friction term has the following relationship [18]:

$$(\Delta P)_{pf} = \alpha u + \beta u^2 \tag{4}$$

where α refers to the viscous permeability effect due to the Stokes flow in the void spaces between the particles, and β accounts for the effect of the pore-scale local inertia. These coefficients have been formulated via empirical models for the packed beds. In this study, one famous empirical formula, known as Ergun's equations, is used, which is applicable to the packed beds with a uniform packing geometry [18]:

$$\alpha \equiv \frac{\mu}{K} = \frac{150\mu(1-\varepsilon)^2}{d_p^2\varepsilon^3} \tag{5}$$

$$\beta \equiv \frac{\rho C}{2} = \frac{1.75\rho(1-\varepsilon)}{d_p\varepsilon^3} \tag{6}$$

where K is defined as the viscous permeability of porous media, C is the inertial coefficient, and d_p is the particle diameter.

3.1. Inertial effect approximation

To deal with the nonlinear inertial effect, a general linearization can be proposed and validated afterward for moderate flowrates ($0 < \mathrm{Re}_p < 300$).

$$(\Delta P)_{vf,inertial} \equiv \beta u^2 \cong \beta(\phi_1 U_0 u) + O(u^2), \text{ where } 0 \leqslant u \leqslant \phi_2 U_0 \tag{7}$$

where U_0 is the average velocity calculated from the inlet flowrate divided by the packed bed cross-sectional area, *i.e.*, $U_0 = Q/A$. The approximation is sub-linear, when $0 < \phi_1 < 1$, and is super-linear, when $\phi_1 > 1$ [39]. The term ϕ_2 varies accordingly in the range of $1 < \phi_2 \leq 2$ from a very low permeability to a full viscous flow condition inside the cylinderical packed beds.

To accurately approximate the nonlinear inertial effect by the linear Eq. (7), an error analysis is required. The local error, $e_u(r)$, at each point along the packed bed cross section can be defined as follows:

$$e_u(r) \equiv u^2(r) - \phi_1 U_0 u(r) \tag{8}$$

By normalizing the local error, one can achieve:

$$\hat{e}_u := \frac{e_u(r)}{U_0^2} = \left(\frac{u}{U_0}\right)^2 - \phi_1\left(\frac{u}{U_0}\right) = \hat{u}^2 - \phi_1\hat{u} \tag{9}$$

where $\hat{u} = u/U_0$. The global L_2 norm of the error in the velocity field will be obtained consequently as:

$$E(\phi_1,\phi_2) := \int_0^{\phi_2} \hat{e}_u^2 d\hat{u} = \phi_2^3\left(\frac{\phi_2^2}{5} + \frac{\phi_1^2}{3} - \frac{\phi_1\phi_2}{2}\right) \tag{10}$$

Considering linearization error in the space of approximating variables (ϕ_1,ϕ_2), the minimized error occurs along $\phi_1 = 3/4\phi_2$ for a given ϕ_2 with $\partial E/\partial\phi_1 = 0$ and $\partial^2 E/\partial\phi_1^2 > 0$. A value of $\phi_2 = 4/3$ is selected within the discussed range of ϕ_2, which simplifies the derived formulas to the linear approximation with $\phi_1 = 1$. A parametric study on the linearization parameters has been performed in Section 6.1.

For an acceptable linear approximation, the maximum norm of error along the radial direction should be bounded:

$$E \equiv \|e_u(r)\|_\infty \equiv \max_{0\leqslant r\leqslant R} |e_u(r)| < \delta, \text{ where } \delta \text{ is finite.} \tag{11}$$

Using Eq. (8) with $\phi_1 = 1$, the maximum error occurs at r_m, where $u(r_m) = U_0/2$. Substituting $u(r_m)$ into Eq. (8), the maximum error is obtained:

$$E \equiv ||e_u(r)||_\infty \leqslant \frac{U_0^2}{4} \approx O(U_0^2) \tag{12}$$

Eq. (12) reveals that, in order to maintain the order of magnitude of the maximum error below unity, the average velocity should be $0 \leq U_0 \leq 1$, which is a valid assumption for the packed beds with moderate inlet air flowrate ($0 < \mathrm{Re_p} < 300$) at $T = 25°C$ and $P = 101.325$ kPa. In this range of particle Reynolds number ($\mathrm{Re_p} = \rho U_0 d_p/\mu$), laminar flow regime is assumed, as the turbulence effects are considered for higher particle Reynolds numbers ($\mathrm{Re_p} > 300$) [40]. By substituting the linear relationship showed in Eq. (7), the overall porous friction term can be rewritten as follows:

$$(\Delta P)_{\mathrm{pf}} \cong \alpha u + \beta U_0 u = (\alpha + \beta U_0)u \tag{13}$$

which can be considered as the linear porous media relation with a modified permeability:

$$\widetilde{K} = \frac{K}{1 + \frac{\beta U_0}{\mu} K} \tag{14}$$

The final linear relation for the porous media can then be simply considered as follows:

$$\frac{1}{\mu}\frac{dP}{dx} = \frac{1}{\varepsilon}\left(\frac{d^2u}{dr^2} + \frac{1}{r}\frac{du}{dr}\right) - \frac{u}{\widetilde{K}} \tag{15}$$

3.2. Analytical solution

To obtain the solution of Eq. (15), the governing equation is non-dimensionalized, using the following reference parameters:

$$\eta = \frac{x}{D},\ \xi = \frac{r}{D},\ u^* = \frac{u}{\frac{1}{\mu}\left(\frac{dP}{dx}\right)D^2},\ \mathscr{Q}^* = \frac{\mathscr{Q}}{\frac{1}{\mu}\left(\frac{dP}{dx}\right)D^4}, \tag{16}$$

where $\mathscr{Q}^*$ is the non-dimensional volumetric flowrate inside the packed bed. The dimensionless differential equation describing the velocity profile inside the packed bed can be written as follows:

$$\Lambda(u^*): = M^*\left(\frac{d^2u^*}{d\xi^2} + \frac{1}{\xi}\frac{du^*}{d\xi}\right) - \frac{u^*}{\widetilde{K}^*} - 1 = 0,\ M^* = \frac{1}{\varepsilon},\ 0 \leqslant \xi \leqslant \frac{1}{2} \tag{17}$$

where the non-dimensional permeability is defined by:

$$\widetilde{K}^* = \frac{K^*}{1 + \left(\frac{D}{d_p}\right)\mathrm{Re}_p K^* C^*} \tag{18}$$

In Eq. (18), the non-dimensional terms are defined based on Ergun's equation [18]:

$$K^* = \frac{\varepsilon^3\left(\frac{d_p}{D}\right)^2}{150(1-\varepsilon)^2},\ C^* = \frac{1.75(1-\varepsilon)}{\left(\frac{d_p}{D}\right)\varepsilon^3} \tag{19}$$

The solution to Eq. (17) with no-slip boundary condition at the wall of the cylinder, *i.e.*, $u^*(1/2) = 0$, and the axisymmetric condition at the center of the cylinder, *i.e.*, $(du^*/d\xi)_{\xi=0} = 0$, is as follows:

$$\frac{u^*(\xi)}{\widetilde{K}^*} = 1 - \frac{I_0(2\lambda\xi)}{I_0(\lambda)},\ \lambda = \frac{1}{2\sqrt{M^*\widetilde{K}^*}} \tag{20}$$

where $I_0(\xi)$ is the modified Bessel function of the first kind, $I_n(\xi) = \sum_{m=0}^{\infty} (\xi/2)^{n+2m}/m!(m+n)!$ [39]. The non-dimensional flowrate inside the bed, $\mathscr{Q}^* = \int_0^{\frac{1}{2}} 2\pi\xi u^*(\xi)d\xi$, can be found as follows:

$$\frac{\mathscr{Q}^*}{\widetilde{K}^*} = \frac{\pi}{4}\left[1 - \frac{2}{\lambda}\frac{I_1(\lambda)}{I_0(\lambda)}\right],\ \lambda = \frac{1}{2\sqrt{M^*\widetilde{K}^*}} \tag{21}$$

Having the dimensionless flowrate of the packed bed, pressure drop in the bed can be obtained by:

$$\frac{\Delta P}{\sigma^2 \mathrm{Re_p}} = \frac{A^*\eta}{\mathscr{Q}^*} \tag{22}$$

where $A^* = \frac{A}{D^2} = \pi/4$ is the dimensionless cross-sectional area of the cylinder, and $\sigma = \mu/(\widetilde{D}\sqrt{\rho})$, where $\widetilde{D} = \sqrt{Dd_p}$. Substituting $\mathscr{Q}^*$ into Eq. (22) gives the final closed form relationship for the pressure drop in a cylindrical granular packed bed, as follows:

$$\frac{\Delta P}{(\sigma^2 \mathrm{Re_p}/\widetilde{K}^*)} = \frac{\eta}{1 - \frac{2I_1(\lambda)}{\lambda I_0(\lambda)}},\ \lambda = \frac{1}{2\sqrt{M^*\widetilde{K}^*}} \tag{23}$$

Combining Eqs. (16), (20), and (23), the macroscopic flow profile can be rewritten as follows:

$$\frac{u(\xi)}{U_0} = \frac{I_0(\lambda) - I_0(2\lambda\xi)}{I_0(\lambda) - \frac{2}{\lambda}I_1(\lambda)} \tag{24}$$

Based on the definition of the parameter $\lambda \equiv \lambda(M^*, \widetilde{K}^*)$ in Eq. (23), higher λ represents lower permeability in the dense porous media, where the velocity profile of the bulk flow tends to have a more uniform distribution. Accordingly, the pattern of the macroscopic flow is affected by changing the modified permeability, $\widetilde{K}^*$, as shown in Eq. (24).

3.3. Asymptotic analysis

Considering both the viscous and porous resistances for obtaining the pressure drop relationship inside the cylindrical packed beds, two asymptotic conditions can be directly derived by the Eq. (23) as follows:

(I) Very low permeability, when $\widetilde{K}^* \to 0$, and $\lambda \to \infty$, which occurs in conventional packed beds with random packing arrangements.
(II) Very high permeability, when $\widetilde{K}^* \to \infty$, and $\lambda \to 0$, which resembles a homogeneous fluid.

Accordingly, the dimensionless pressure drop can be expressed as follows:

$$f(\lambda) = \frac{\Delta P}{\sigma^2 \mathrm{Re_p} M \eta} = \frac{4\lambda^2}{1 - \frac{2}{\lambda}\left(\frac{I_1(\lambda)}{I_0(\lambda)}\right)} \tag{25}$$

For the first asymptote, $\widetilde{K}^* \to 0$, the following solution can be found:

$$f(\lambda) \approx 4\lambda^2, \text{ as } \lambda \to \infty \tag{26}$$

Therefore, the pressure drop of a cylindrical packed bed can be obtained as:

$$\frac{\Delta P}{\sigma^2 \mathrm{Re_p}} = \frac{\eta}{\widetilde{K}^*} \tag{27}$$

Substituting Eq. (19) into Eq. (27), Ergun's equation can be derived for the pressure drop inside the porous media. Eq. (27) reveals that at the upper limit, the viscous friction term has negligible effect, and consequently, the pressure drop is not affected by the geometry of the packed bed. Conversely, for a very high permeability asymptote, which resembles a near homogenous fluid condition, $f(\lambda)$ reaches to 32, which is the solution of homogenous Poiseuille fluid flow in a cylindrical pipe [18], *i.e.*:

$$f(\lambda) \approx 32, \text{ as } \lambda \to 0 \tag{28}$$

In this case, the total pressure drop depends only on fluid dynamic viscosity, flowrate, and the bed geometry, as follows:

$$\frac{\Delta P}{QH} = \frac{128\mu}{\pi D^2} \tag{29}$$

Consequently, an intermediate condition can be observed between

these two asymptotes using Eq. (25), where both fluid viscosity and porous resistance are equally important. This condition can occur in artificially designed (ordered) packed beds with relatively high permeability. It will be described in more details in the results and discussion section.

4. CFD simulation of pressure drop

A CFD simulation is also performed to analyze the validity of the proposed semi-analytical model. The governing equations for an incompressible steady isothermal fluid flow inside the porous media are modeled via an axisymmetric frame. The momentum-pressure coupling problem is solved by SIMPLE algorithm, through *porousSimpleFoam* solver provided in OpenFOAM-3.0.1 [41]. A structured uniform grid is used to discretize the domain. *Wedge* boundary condition is employed to transfer a 3D mesh to an axisymmetric 2D mesh. The mesh is provided by *blockMesh* facility of the OpenFOAM. The parameters of Darcy-Forchheimer porous media model [42] is determined based on Eqs. (5) and (6). The turbulence effects are neglected since the particle Reynolds number in the domain is low ($Re_p < 300$). The initial value for the fluid velocity is equal to the inlet velocity, and the iterations to the numerical solution are continued until the prescribed convergence criteria are met ($|\delta_e| \leqslant 10^{-12}$, where δ_e is the change to the field variable between the iterations).

A uniform fixed-value velocity and a zero-gradient pressure are considered at the inlet and a zero-gradient velocity and a fixed-value zero pressure conditions are set at the outlet. By implementing wedge boundary condition, the circumferential variation is neglected and an axisymmetric 2D solution is provided. A grid study has been done on the solution accuracy. Accordingly, mesh configurations of 40×120 and 40×320 are found as the optimal grid sizes for the bed heights of 12 and 30 cm, respectively. The first and second numbers in these mesh configurations are the number of the computational cells along the radial (r) and azimuthal (x) directions, respectively.

The convective terms are discretized by the upwind scheme. The flux of variables on a face is obtained by a linear interpolation of the adjacent cells to the face. The pressure equation is solved by algebraic multi-grid scheme, while the momentum equation is solved by a Gauss-Seidel algorithm [33]. For increasing the stability of the SIMPLE solver, relaxation factors of 0.3 and 0.7 are used for the pressure and momentum equations, respectively [33].

5. Experimental study

A testbed including a cylindrical container with the inner diameter of 7.62 cm (3.0 in) and the height of 30 cm was designed and built as a laboratory-scale packed bed, shown in Fig. 2. The container was filled with two different adsorbent materials, silica gel and zeolite 4A, with different heights, and connected to a wind tunnel, which provided different air flowrates. The porosity of the packed bed was 0.375 and 0.39 for silica gel and zeolite particles, respectively. A calming section was considered before the inlet of the adsorption packed bed to provide a uniform air velocity. To measure the pressure drop along the porous packed bed, a differential pressure transducer (Setra-267w) with accuracy of ± 1.0% full scale (± 12.5 Pa) was used. The pressure drop was measured for the packed bed with different silica gel heights of 6, 12, 18, 24, and 30 cm.

Table 1
Testbed conditions for pressure drop measurements.

Adsorbent	Porosity	Particle diameter	Column height	Airflow velocity	Initial condition
Silica gel	0.375	3.2 mm	6–30 cm	0.13–0.83 m/s	dry (zero uptake)
Zeolite 4A	0.39	3.6 mm	6–30 cm	0.13–1.03 m/s	dry and wet

The inlet air temperature was 23 °C and the relative humidity was 55% during the course of the experiments. For dry adsorbent case, the pressure drop was measured at the beginning of the experiment. To ensure the repeatability of the results, each experiment was repeated at least three times with dry silica gel particles under a constant packed bed height. The maximum uncertainty for the pressure drop measured along the packed bed with 30 cm height was 11.3%. To investigate the effect of uptake on the pressure drop, the bed filled with completely wet zeolite was studied as well. Further information about the test conditions are presented in Table 1.

6. Results and discussion

Fig. 3 compares the analytical, experimental, and CFD simulation data for different inlet air velocity and desiccant column heights. As shown, there is a good agreement between the present results and the experimental data; at the maximum inlet air velocity, the relative difference between the analytical results and the measured experimental data is 7.6% at air velocity of 0.73 m/s for silica gel, and 15.3% at 0.84 m/s for zeolite beds. The averaged uncertainty of the measurement is estimated as 4.92% for the silica gel bed and 4.74% for the zeolite bed. The CFD model shows a 7.08% deviation from the experimental data at the maximum inlet velocity and perfectly matches with the analytical results with 0.48% difference. This indicates consistency between the analytical results, the experimental data, and the numerical solution.

Fig. 4 compares the pressure gradient along the bed, dP/dx, calculated by the present model with the experimental data of randomly-

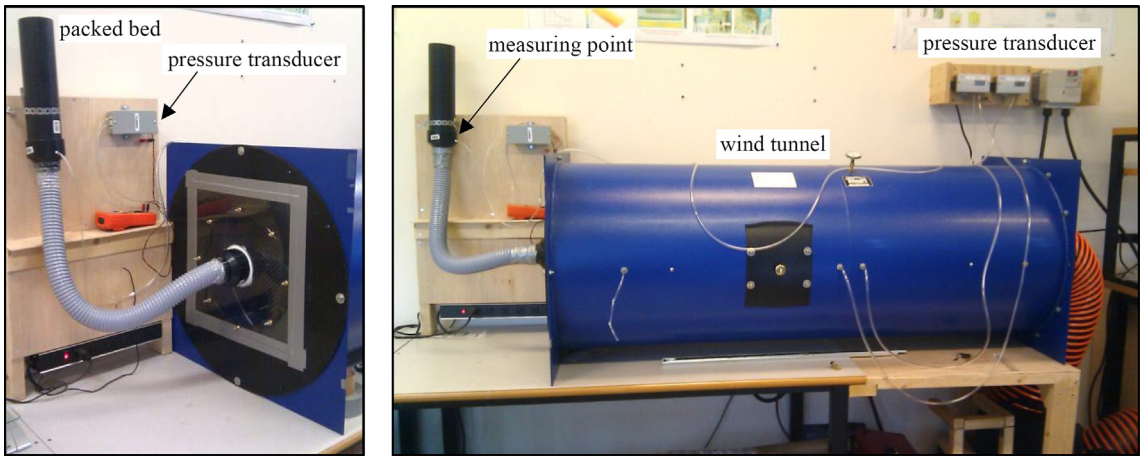

Fig. 2. Experimental testbed for pressure drop measurements in the cylindrical packed bed.

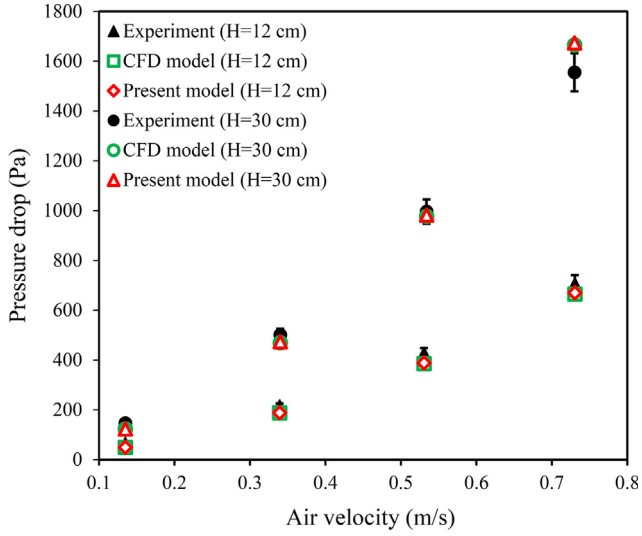

Fig. 3. Comparison of the analytical model with the CFD simulation and experiments for the cylindrical packed column of silica gel with different heights.

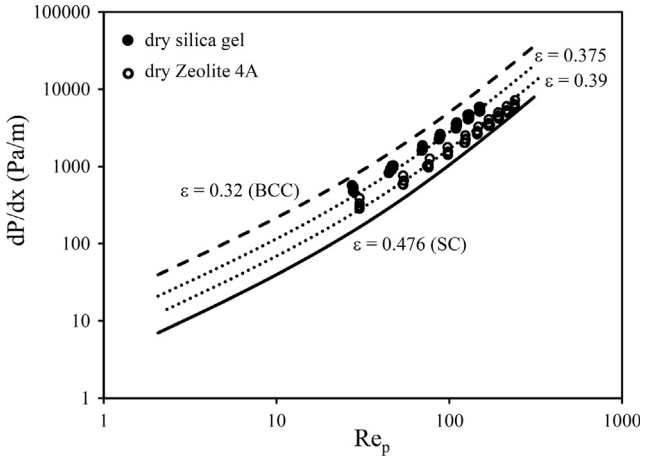

Fig. 4. Pressure gradient along the packed bed for different packing arrangements compared to the proposed analytical model, Eq. (22).

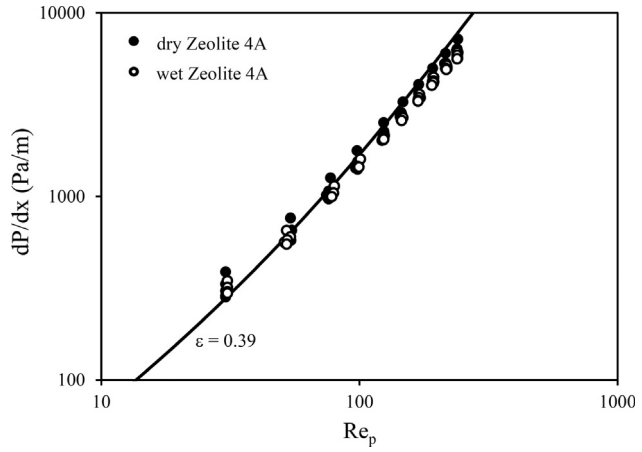

Fig. 5. Comparison of dry and wet zeolite particles for pressure gradient along the packed bed.

packed bed of dry silica gels with a porosity of $\varepsilon = 0.375$ and dry zeolite 4A with a porosity of $\varepsilon = 0.39$. Other packing arrangements, *i.e.* simple cubic (SC) and body centered cubic (BCC) [43] are also added for comparison.

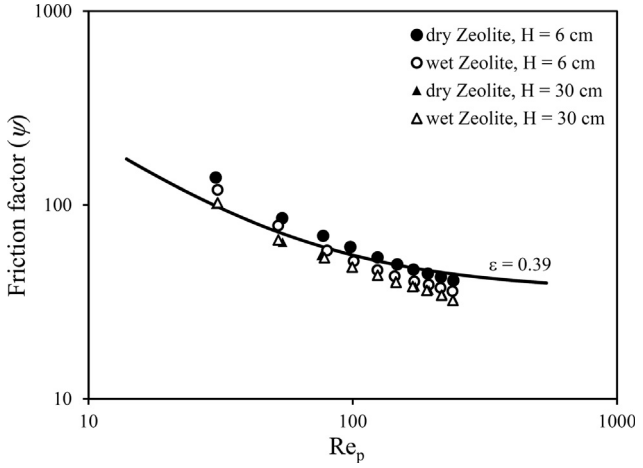

Fig. 6. Comparison of dry and wet zeolite particles with analytical model for the friction factor.

Table 2
The effect of water uptake on pressure drop in wet with respect to dry zeolite 4A for different column sizes.

Bed height (cm)	Total pressure difference, $\Delta P = P_d - P_w$ (Pa)	Pressure difference per bed height, $\Delta P/H$ (Pa/cm)	Relative pressure difference, $(P_d - P_w)/P_d$ (%)	Relative friction factor difference, $(f_d - f_w)/f_d$ (%)
6	57.5	9.58	12.50	13.03
18	29.2	1.62	3.02	4.05
30	54.2	1.81	0.82	0.29

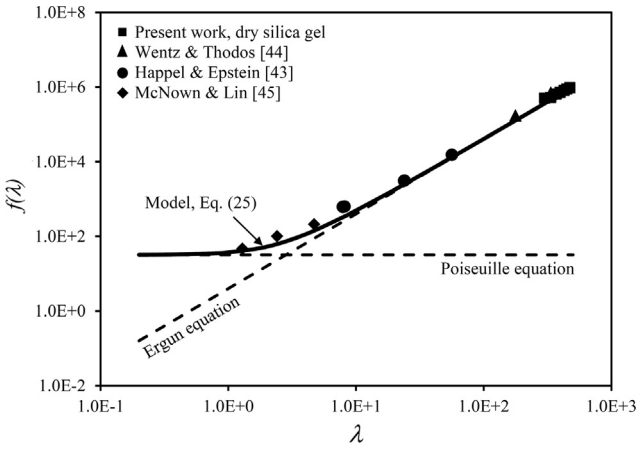

Fig. 7. Comparison of the present analytical model with the present experiments, as well as the available experimental data in the literature [43,44,45], for different range of permeability.

Table 3
Sorption characteristics of adsorbents for ideal energy storage density calculation, considering the experimental conditions of $T = 23°C$ and $RH = 55\%$. (the maximum water uptake is defined as the maximum mass of the adsorbed water to the mass of the dry adsorbent).

Adsorbent	Enthalpy of adsorption (ΔH_{ads})	Maximum uptake (w_{max})
Silica gel	2.40 MJ/kg [47]	0.40 kg/kg_{ads} [49]
Zeolite 4A	3.05 MJ/kg [47]	0.22 kg/kg_{ads} [50]

As shown in Fig. 4, pressure gradients of the tested desiccants lie between SC and BCC arrangements. Accordingly, for a given particle Reynolds number, the pressure gradient along the bed reduces at

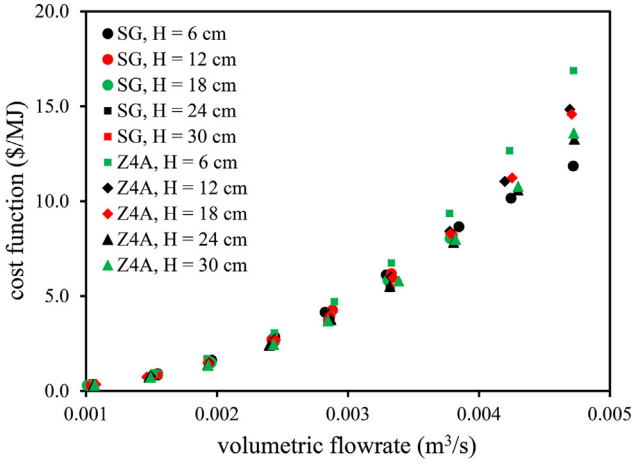

Fig. 8. Operational cost function for annual operation of silica gel (SG) and zeolite 4A (Z4A) adsorber bed.

packing arrangements with higher porosities. To investigate the effect of the uptake on the pressure drop, a series of experiments have been performed for fully wet zeolite packed bed and the results were compared to the results obtained from the experiment with dry zeolite. Fig. 5 compares the pressure gradient along the bed of dry and wet zeolite 4A with the analytical model. As shown in this figure, the pressure drop for the wet particles did not change significantly compared to the dry particles.

Fig. 6 compares the analytical results for the friction factor, defined in Eq. (30), for the analytical model with the experiment data of dry and wet zeolite 4A for the cylindrical packed bed.

$$\psi = \frac{\Delta P}{\frac{1}{2}\rho U_0^2}\left(\frac{d_p}{H}\right) \tag{30}$$

As shown in Fig. 6, the differences between dry and wet desiccants become negligible as the column size increases. A maximum of about 12% relative pressure difference was observed in the experiments for the wet particles in 6 cm bed height versus the dry particles; while in 30 cm bed height, the maximum relative difference was less than 1%. Table 2 shows the maximum differences in dry and wet conditions. According to this table, insignificant pressure differences per adsorber bed height can be observed at slightly larger beds ($H > 6.0$ cm). This was also found for relative pressure and friction factor differences.

As shown in Fig. 7, an intermediate condition can be observed between one asymptote (very low permeability) and another asymptote (very high permeability) by increasing the porosity of packed bed from

Table 4
The effect of linearization variable along $\phi_1 = 3/4\phi_2$ with $0.5 < \phi_1 < 1.5$ on the modified permeability, $\widetilde{K}^*$, as well as deviations of modified permeability from the viscous permeability, K^* ($\widetilde{K}^*_{0,1.5} = \widetilde{K}^*(\phi_1 = 0.5,1.5)$).

Particle Reynolds number (Re_p)	Permeability ratio		
	$\widetilde{K}^*_{0.5}/\widetilde{K}^*$	$\widetilde{K}^*_{1.5}/\widetilde{K}^*$	$\widetilde{K}^*/K^*$
10	1.081	0.927	0.843
50	1.297	0.805	0.517
100	1.448	0.754	0.349

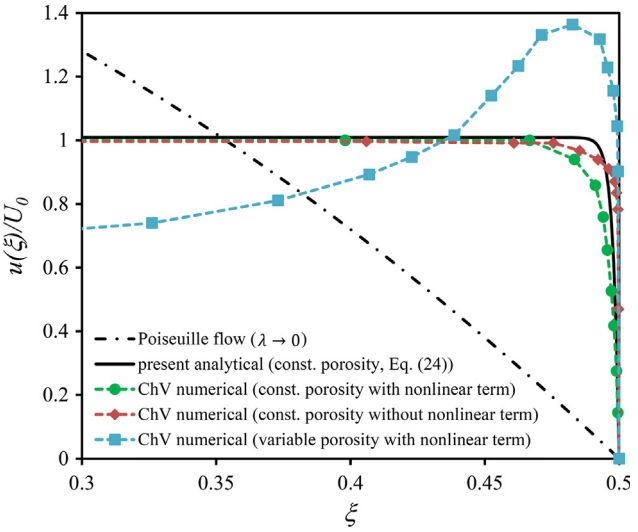

Fig. 10. Comparison of present model with numerical results of Chandrasekhara and Vortmeyer (ChV) [51] for constant and variable porosity ($\varepsilon_0 = 0.4$, $Re_p = 84$, $U_0 = 0.3078$ m/s, $d_p = 6.35$ mm, $D = 5$ cm, $\lambda = 234$).

high to low λ. According to this figure, the intersection of the two asymptotes occurs at $\lambda = 2\sqrt{2}$, where the maximum deviation from both asymptotes occurs.

To reflect the effect of pressure drop on the storage properties, the fan operational cost function can be introduced, similar to the definition used in Ref. [46], as follows:

$$CF_{operational,fan} = \frac{C_{electricity}\Delta P(\dot{m}_{air}/\rho_{air})\Delta t_{operational}}{ESD_{ideal} \times V_{sys}}\,[\$/MJ] \tag{31}$$

where $C_{electricity}$ [$/kWh]is the electricity price and ESD_{ideal} is the ideal energy storage density of the adsorption packed bed, which can be

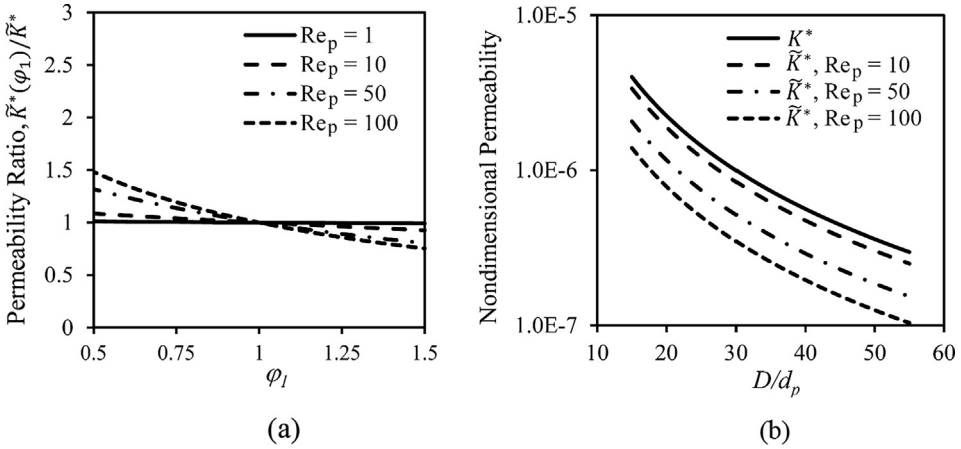

Fig. 9. Variation of $\widetilde{K}^*$ as a modification to the packed bed's permeability for different particle Reynolds number, (a) with respect to the linearization variable, ϕ_1, (b) deviation from viscous permeability.

Table 5
Estimation of temperature effect on pressure drop using present analytical model for adsorber beds with $H = 30$ cm (T_0, RH_0, and $\delta_x = (x-x_0)/x_0$ are inlet temperature, inlet relative humidity, and relative difference of x, respectively).

Adsorbent	U_0 (m/s)	T_0 (°C)	RH_0 (%)	$\Delta P_{exp,dry}$ (kPa)	ΔP_{model} (kPa)	ΔT_{max} (°C)	δ_ρ (%)	δ_μ (%)	$\delta_{\Delta P,model}$ (%)
Silica gel	0.34	25	92	0.501 ± 0.025	0.473	+25.3	−7.8	+6.2	−1.3
Zeolite 4A	0.13	26	85	0.085 ± 0.004	0.083	+33.8	−10.2	+8.7	+1.7

calculated based on the sorption properties of adsorbents [47]:

$$ESD_{ideal} = \rho_s w_{max} \Delta H_{ads} \quad (32)$$

where ρ_s is the apparent density of the adsorbent, w_{max} is the maximum net uptake capacity based on the equilibrium isotherm and operating conditions, and ΔH_{ads} is the enthalpy of adsorption. The corresponding values are presented in Table 3. The averaged electricity price for a Canadian household in 2017 is considered as $C_{electricity} = 0.1265$$/kWh (Canadian dollar) [48]. Fig. 8 shows the calculated cost function for the annual operation versus the air flowrate for silica gel and zeolite 4A adsorber bed in the present study.

6.1. Parametric study

Fig. 9(a) shows the variation of the modified permeability, $\widetilde{K}^*$, as a function of the linearization parameter, ϕ_1, along the minimized error line, $\phi_1 = 3/4\phi_2$, discussed in Section 3.1.

$$\widetilde{K}^*(\phi_1) = \frac{K^*}{1 + \left(\frac{D}{d_p}\right) \mathrm{Re}_p \phi_1 K^* C^*} \quad (33)$$

It can be seen from Fig. 9(a) that the modified permeability deviates considerably from the linear condition ($\phi_1 = 1$) as the particle Reynolds number increases. A relative change of 10% occurs for $\mathrm{Re_p} = 100$ within the range of $\phi_1 = 1.0 \pm 0.15$. This relative change decreases by reducing $\mathrm{Re_p}$. The deviations in the modified permeability, $\widetilde{K}^*(\phi_1)/\widetilde{K}^*$, are presented in Table 4 for $0.5 < \phi_1 < 1.5$.

Moreover, the modified permeability changes with bed-to-particle diameter, D/d_p, and the particle Reynolds number, $\mathrm{Re_p}$, for a fixed porosity, $\varepsilon = 0.375$, in Fig. 9(b). For a specified bed and particle geometries, increasing the particle Reynolds number decreases the modified permeability, $\widetilde{K}^*$, which results in higher flow resistance associated with higher inertial effects in packed beds. Deviations from the viscous permeability, $\widetilde{K}^*/K^*$, are presented in Table 4 for different particle Reynolds number.

Fig. 10 compares the analytical velocity profile, Eq. (24), with the numerical work of Chandrasekhara & Vortmeyer [51]. For the constant porosity case, both analytical and numerical solutions show a uniform velocity distribution with a thin layer of high gradient near the wall, due to the no-slip condition. Moreover, the effect of porosity variation near the wall [28], which causes local flow channeling, can be observed by numerical solution of Chandrasekhara & Vortmeyer [51].

Due to the heat of adsorption, a temperature change in the adsorber packed bed occurs, which affects the adsorbate (air) density and viscosity. To see the thermal effects, the bed's outlet temperature was measured during the adsorption process. Using the analytical model, Table 5 shows a maximum change of up to ± 2% for pressure drop, although a considerable air temperature lift (*i.e.* 25.3 °C for silica gel and 33.8 °C for zeolite 4A) occurs.

7. Conclusion

A new analytical model was proposed for calculating the pressure drop in a cylindrical packed bed with laminar, steady-state, axisymmetric, and fully-developed macroscopic fluid flow distributions. The Laplacian friction and inertial effect were introduced to the analytical model, and the effect of these terms on the pressure drop inside the packed beds was investigated. A modified permeability was defined which contained the inertial effect for moderate range of particle Reynolds number ($0 < Re_p < 300$). It was shown that the proposed model covered a wide range of permeability and properly predicted an intermediate condition, where the flow distribution inside the bed shifted gradually from a near homogenous fluid with viscous dominant condition to a conventional packed bed with porous resistance effects, as the main cause of the pressure loss along the packed bed.

An experimental study was performed to validate the proposed analytical model. Moreover, a CFD simulation based on the steady-state incompressible isothermal air flow was performed to study numerically the pressure drop inside the packed bed. The relative difference for the analytical solution with respect to the experimental data of dry silica gel was 7.6% at the maximum inlet air velocity, while the CFD model showed a 7.08% deviation from the experimental data, which showed a proper consistency between the analytical results, the numerical solution, and the measured pressure drop.

The effect of uptake on the pressure drop in the ATES was investigated experimentally through testing completely dry and fully wet zeolite packed bed. It was concluded that as the pressure drop increases, the relative difference in the pressure drop between the dry and wet beds is negligible. Therefore, the proposed analytical formula for the dry zeolite packed bed can be implemented to the partially or completely wet zeolite packed bed, as a good approximation.

Considering porosity variation near the wall is a complementary work to the proposed model, which can analytically formulate the effect of flow channeling adjacent to the wall on the velocity distribution and the pressured drop inside the adsorption packed bed thermal energy storage systems.

Acknowledgments

The authors gratefully acknowledge the financial support of the Natural Sciences and Engineering Research Council of Canada (NSERC) through the Automotive Partnership Canada Grant No. APCPJ 401826-10.

References

[1] J. Nastaj, B. Ambrozek, Modeling of drying of gaseous mixtures in TSA system with fixed bed of solid desiccants, Dry. Technol. 30 (10) (2012) 1062–1071.
[2] M. Ncube, Y. Su, The removal of volatile organic compounds from supply air using a desiccant column - A theoretical study, Int. J. Sustain. Built Environ. 1 (2) (2012) 259–268.
[3] A.K. Ramzy, R. Kadoli, T.P. Ashok Babu, Experimental and theoretical investigations on the cyclic operation of TSA cycle for air dehumidification using packed beds of silica gel particles, Energy 56 (2013) 8–24.
[4] M.J. Tuinier, M.V.S. Annaland, Biogas purification using cryogenic packed-bed technology, 2012.
[5] A. Sharafian, M. Bahrami, Assessment of adsorber bed designs in waste-heat driven adsorption cooling systems for vehicle air conditioning and refrigeration, Renew. Sustain. Energy Rev. 30 (2014) 440–451.
[6] A. Hauer, Evaluation of adsorbent materials for heat pump and thermal energy storage applications in open systems, Adsorption 13 (3–4) (2007) 399–405.
[7] A. Solé, I. Martorell, L.F. Cabeza, State of the art on gas-solid thermochemical energy storage systems and reactors for building applications, Renew. Sustain. Energy Rev. 47 (2015) 386–398.
[8] R. Anderson, L. Bates, E. Johnson, J.F. Morris, Packed bed thermal energy storage: A simplified experimentally validated model, J. Energy Storage 4 (2015) 14–23.
[9] X. Cheng, X. Zhai, R. Wang, Thermal performance analysis of a packed bed cold storage unit using composite PCM capsules for high temperature solar cooling application, Appl. Therm. Eng. 100 (2016) 247–255.

[10] H. Zondag, B. Kikkert, S. Smeding, R. de Boer, M. Bakker, Prototype thermochemical heat storage with open reactor system, Appl. Energy 109 (2013) 360–365.
[11] D. Aydin, S.P. Casey, S. Riffat, The latest advancements on thermochemical heat storage systems, Renew. Sustain. Energy Rev. 41 (2015) 356–367.
[12] A. Hauer, F. Fischer, Open adsorption system for an energy efficient dishwasher, Chemie-Ingenieur-Technik 83 (1–2) (2011) 61–66.
[13] H. Schreiber, S. Graf, F. Lanzerath, A. Bardow, Adsorption thermal energy storage for cogeneration in industrial batch processes: experiment, dynamic modeling and system analysis, Appl. Therm. Eng. 89 (2015) 485–493.
[14] S.K. Yeboah, J. Darkwa, A critical review of thermal enhancement of packed beds for water vapour adsorption, Renew. Sustain. Energy Rev. 58 (2016) 1500–1520.
[15] H. Kerskes, B. Mette, F. Bertsch, S. Asenbeck, H. Drück, Chemical energy storage using reversible solid/gas-reactions (CWS) - Results of the research project, Energy Procedia 30 (2012) 294–304.
[16] M. Kaviany, Principles of Heat Transfer in Porous Media, 1st ed., Springer-Verlag, New York, 1991.
[17] K.G. Allen, T.W. von Backström, D.G. Kröger, Packed bed pressure drop dependence on particle shape, size distribution, packing arrangement and roughness, Powder Technol. 246 (2013) 590–600.
[18] S. Ergun, A.A. Orning, Fluid Flow through Randomly Packed Columns and Fluidized Beds, Ind. Eng. Chem. 41 (6) (1949) 1179–1184.
[19] J.S. Andrade, U.M.S. Costa, M.P. Almeida, H.A. Makse, H.E. Stanley, Inertial effects on fluid flow through disordered porous media, Phys. Rev. Lett. 82 (26) (1999) 5249–5252.
[20] M. Veyskarami, A.H. Hassani, M.H. Ghazanfari, Modeling of non-Darcy flow through anisotropic porous media: Role of pore space profiles, Chem. Eng. Sci. 151 (2016) 93–104.
[21] T. Atmakidis, E.Y. Kenig, CFD-based analysis of the wall effect on the pressure drop in packed beds with moderate tube/particle diameter ratios in the laminar flow regime, Chem. Eng. J. 155 (1–2) (2009) 404–410.
[22] P. Kundu, V. Kumar, I.M. Mishra, Numerical modeling of turbulent flow through isotropic porous media, Int. J. Heat Mass Transf. 75 (2014) 40–57.
[23] L.W. Rong, K.J. Dong, A.B. Yu, Lattice-Boltzmann simulation of fluid flow through packed beds of uniform spheres: Effect of porosity, Chem. Eng. Sci. 99 (2013) 44–58.
[24] A. Tamayol, M. Bahrami, Analytical determination of viscous permeability of fibrous porous media, Int. J. Heat Mass Transf. 52 (9–10) (2009) 2407–2414.
[25] A. Tamayol, M. Bahrami, Transverse permeability of fibrous porous media, Phys. Rev. E - Stat. Nonlinear, Soft Matter Phys. 83 (4) (2011) 1–9.
[26] H.C. Brinkman, A calculation of the viscous force exerted by a flowing fluid on a dense swarm of particles, Appl. Sci. Res. 1 (1) (1949) 27–34.
[27] G.H. Neale, W.K. Nader, Prediction of transport processes within porous media: diffusive flow processes within an homogeneous swarm of spherical particles, AIChE J. 19 (1) (1973) 112–119.
[28] A. De Klerk, Voidage variation in packed beds at small column to particle diameter ratio, AIChE J. 49 (8) (2003) 2022–2029.
[29] L. Pistocchini, S. Garone, M. Motta, Porosity and pressure drop in packed beds of spheres between narrow parallel walls, Chem. Eng. J. 284 (2016) 802–811.
[30] P. Finocchiaro, M. Beccali, V. Gentile, Experimental results on adsorption beds for air dehumidification, Int. J. Refrig. 63 (2016) 100–112.
[31] F. Opitz, P. Treffinger, Packed bed thermal energy storage model – Generalized approach and experimental validation, Appl. Therm. Eng. 73 (1) (2014) 243–250.
[32] M. Cascetta, G. Cau, P. Puddu, F. Serra, A comparison between CFD simulation and experimental investigation of a packed-bed thermal energy storage system, Appl. Therm. Eng. 98 (2016) 1263–1272.
[33] J.H. Ferziger, M. Peric, Computational Methods for Fluid Dynamics, 3rd ed., Springer-Verlag, Berlin Heidelberg, 2002.
[34] A. Ramzy K, T.P. Ashok Babu, R. Kadoli, Semi-analytical method for heat and moisture transfer in packed bed of silica gel, Int. J. Heat Mass Transf. 54 (4) (2011) 983–993.
[35] A. Hauer, L. Eberhardt, Open absorption systems for air conditioning and thermal energy storage, in: thermal energy storage for sustainable energy consumption, 2007, pp. 429–444.
[36] A. Freni, L. Bonaccorsi, L. Calabrese, A. Caprì, A. Frazzica, A. Sapienza, SAPO-34 coated adsorbent heat exchanger for adsorption chillers, Appl. Therm. Eng. 82 (2015) 1–7.
[37] A. Freni et al., Characterization of Zeolite-Based Coatings for Adsorption Heat Pumps, first ed. Springer International Publishing, 2015.
[38] D.A. Nield, A. Bejan, Convection in Porous Media, 5th ed., Springer-Verlag, New York, 2017.
[39] D. Levy, Introduction to Numerical analysis, 2010.
[40] B. Eisfeld, K. Schnitzlein, The influence of confining walls on the pressure drop in packed beds, Chem. Eng. Sci. 56 (14) (2001) 4321–4329.
[41] C.J. Greenshields, OpenFOAM User Guide 3.0.1, no. December, 2015.
[42] Z. Zeng, R. Grigg, A criterion for non-darcy flow in porous media, Transp. Porous Media 63 (1) (2006) 57–69.
[43] J. Happel, N. Epstein, Cubical assemblages of uniform spheres, Ind. Eng. Chem. 46 (6) (1954) 1187–1194.
[44] C.A. Wentz, G. Thodos, Pressure drops in the spherical particles flow of gases through packed and distended beds of spherical particles, AIChE J. 9 (1) (1963) 81–84.
[45] J.S. McNown, P.N. Lin, Sediment concentration and fall velocity, in: Second Midwestern Conference on Fluid Mechanics, 1952, pp. 401–411.
[46] L. Scapino, H.A. Zondag, J. Van Bael, J. Diriken, C.C.M. Rindt, Energy density and storage capacity cost comparison of conceptual solid and liquid sorption seasonal heat storage systems for low-temperature space heating, Renew. Sustain. Energy Rev. 76 (March) (2017) 1314–1331.
[47] Y.I. Aristov, Current progress in adsorption technologies for low-energy buildings, Futur. Cities Environ. 1 (1) (2015) 10.
[48] Hydro-Québec, Comparison of electricity prices in major north american cities, Apr. 2017.
[49] H.T. Chua, K.C. Ng, A. Chakraborty, N.M. Oo, M.A. Othman, Adsorption characteristics of silica gel + water systems, J. Chem. Eng. Data 47 (5) (2002) 1177–1181.
[50] A. Gorbach, M. Stegmaier, G. Eigenberger, Measurement and modeling of water vapor adsorption on Zeolite 4A – Equilibria and kinetics, Adsorption 10 (1) (2004) 29–46.
[51] B.C. Chandrasekhara, D. Vortmeyer, Flow model for velocity distribution in fixed porous beds under isothermal conditions, Wärme- und Stoffübertragung 12 (2) (1979) 105–111.